Vision, Modeling, and Visualization (2013)
Michael Bronstein, Jean Favre, and Kai Hormann (Eds.)

Visualization and Analysis of Lumbar Spine Canal Variability in Cohort Study Data

P. Klemm[1], K. Lawonn[1], M. Rak[1], B. Preim[1], K. Toennies[1], K. Hegenscheid[2], H. Völzke[2], S. Oeltze[1]

[1]Otto-von-Guericke University Magdeburg, Germany
[2]Ernst-Moritz-Arndt-University Greifswald, Germany

Abstract

Large-scale longitudinal epidemiological studies, such as the Study of Health in Pomerania (SHIP), investigate thousands of individuals with common characteristics or experiences (a cohort) including a multitude of socio-demographic and biological factors. Unique for SHIP is the inclusion of medical image data acquired via an extensive whole-body MRI protocol. Based on this data, we study the variability of the lumbar spine and its relation to a subset of socio-demographic and biological factors. We focus on the shape of the lumbar spinal canal which plays a crucial role in understanding the causes of lower back pain.
We propose an approach for the reproducible analysis of lumbar spine canal variability in a cohort. It is based on the centerline of each individual canal, which is derived from a semi-automatic, model-based detection of the lumbar spine. The centerlines are clustered by means of Agglomerative Hierarchical Clustering to form groups with low intra-group and high inter-group shape variability. The number of clusters is computed automatically. The clusters are visualized by means of representatives to reduce visual clutter and simplify a comparison between subgroups of the cohort. Special care is taken to convey the shape of the spinal canal also orthogonal to the view plane. We demonstrate our approach for 490 individuals drawn from the SHIP data. We present preliminary results of investigating the clusters with respect to their associated socio-demographic and biological factors.

Categories and Subject Descriptors (according to ACM CCS): J.3 [Computer Applications]: Life and Medical Sciences—Health

1. Introduction

Exploiting the full potential of huge information spaces created by cohort studies like the Study of Health in Pomerania (SHIP) is one of the major challenges in modern epidemiology. The SHIP [VAS*11] aims at characterizing health by assessing data relevant to prevalence and incidence of diseases and identifying their risk factors. With the recent incorporation of medical image data in cohort studies, shape and texture of organs may be characterized. Shape information linked to other medical or lifestyle data show great promise for better understanding of risk factors for certain diseases [WP03]. For example, how does a physically hard job influence the shape of the spine? Scientific findings yield in precise precautions for people who belong to risk groups.

Our focus is on the lumbar spine, which is most often the source of musculoskeletal disorders in clinical practice [vTKB02, WP03]. The whole-body MRI scans of the SHIP are the basis for our approach to enable a reproducible analysis of the lumbar spine canal variability. Our contributions are:

- generation of groups of individuals sharing a similar shape of the lumbar spine canal,
- visualization of these groups by means of representatives,
- illustration of 3D shape in a 2D view.

While the processing of the 490 data sets represents first results, we were able to observe the expected behavior like decreasing spine curvature with increasing subject body height. We also found unexpected clusters of unusual shape, which are now subject to further epidemiological analysis.

2. Related Work

To the best of our knowledge, only Steenwijk and colleagues concurrently query and visualize both image and non-image

DOI: 10.2312/PE.VMV.VMV13.121-128

data in a Visual Analytics framework [SMvB*10]. They put emphasis on a structured data organization and employ a relational database. Their work is closest to ours albeit our investigation of image and non-image data is at the moment still being performed sequentially.

Non-image Data. Cohort study data is often very heterogeneous. It consists of image and non-image data, different types of parameters, e.g. ordinal, nominal, and quantitaive, and parameters of the same type but having different domains, which may partially overlap. Schulze-Wollgasts [SWST03] work supports the data exploration process and hypotheses generation by dividing the information space into data cubes, which can then be understood as n-dimensional arrays. They are used to investigate normalized parameters of different modalities and individuals. Linking & brushing is used to investigate interesting details in the resulting spaces. Zhang and colleagues [ZGP12] extended this approach by a web-based system which allows for grouping of subjects based on associated data variables and feeding groups into a visualization system to support insight into complex correlations of the data attributes. Groups are precomputed by calculating common sets of risk factors. This can serve as starting point for an exploratory analysis. We adapt this approach by computing clusters based on shape.

Image Data. Caban and colleagues [CRY11] give an overview on how shape distribution models can be compared using different methods like deformation grids, likelihood volumes and glyphs. Their presented study favors a spherical glyph representation of variation modes. Busking and colleagues [BBP10] proposed a method which plots instances of a structure on a 2D plane. The user can then generate interpolated views in an object space view via mesh morphing on a reference structure together with a color-coded deformation field on the surface. In the shape evolution view, 2D projections of all structure instances can be compared. With pairwise corresponding data points their segmentation model is of the same type as our spine detection model. Their methods, however, focuses largely on local structural changes while we address curvature. Visualizing our data with their open source `ShapeSpaceExplorer` lead to a very cluttered view, since it is not suited for a large number of input objects. We do not use their approach of main variation modes, since they also display models by interpolating between standard deviation steps, which are not part of the data. Hermann and colleagues [HSK11] compared statistical deformation models to detect anatomically different individuals of the rodent mandibles. They propose a semantically driven user-centered pipeline that includes expert knowledge as region-of-interest selection via interactive volume deformation. This takes especially into account that not all shape information in a model is of equal interest to the user. Chou and colleagues [CLA*09] investigated the correlation of Alzheimer's disease for 240 subjects with ventricular expansion, clinical characteristics, cognitive values and related biomarker by statistically linking them together and ploting their p-values onto the ventricle surface. This way of directly mapping disease-related biomarkers is an example of how different data modalities can be expressively combined. A visual analytics approach for improving model based segmentation is presented by von Landesberger and colleagues [vLBK*13]. They introduced expert knowledge via visual analytics tools into every important step of segmentation from pre-processing to evaluation.

Using deformation fields that describe dense correspondences, Rueckert and colleagues [RFS03] constructed an atlas of average anatomy with variability across a population. Registration-based statistical deformation models are shown to be suitable for characterizing shape over many subjects.

3. Epidemiology of Back Disorders

Epidemiological cohort studies aim to identify factors which are associated with diseases and mortality risks. This includes socio-economic characteristics and medical parameters. While the understanding of genetic mutations regarding back disorders made progress, the correlations with different environmental factors as well as physical stress are not sufficiently understood [MM05]. Manek and colleagues reviewed the progress made in understanding causes of back pain and present influencing factors like age, gender, weight and different lifestyle aspects, such as smoking behavior and work conditions. Tucer and colleagues [TYO*09] conclude that depression is one of the independent risk factors for experiencing low back pain, although their analysis is based on surveys of the subjects and does not rest upon clinical analysis. Lang-Tapia and colleagues [LTERAC11] used a non-invasive method for analyzing spine curvature using a so-called "Spine-Mouse". They correlated spine curvature with age, gender, and weight-status. They did not find correlations between lumbar spine deformation and weight status. Van Tulder and colleagues [vTKB02] conclude that the value of such identified risk factors as prognostic value remains low. No factor arose as strong indication for back pain through many different studies.

These studies share the relation to socio-demographic and medical attribute data with most cohort studies that analyze back disorders. Many studies do not include shape information, only very few use medical imaging at all. One distinct feature of the SHIP are the whole-body MRI scans gathered for a large cohort of 3,368 subjects [HSS*13]. Radiation acting on subjects makes CT imaging ethically unjustifiable. Body-imaging allows for linking the spine shape to other attributes. Spines can be divided into groups to evaluate their potential to induce a pathology. Future cohort assessments even allow to determine change of spine shape.

4. Image Data Acquisition and Spine Detection

All whole-body MRI scans were acquired on a 1.5 Tesla scanner (Magnetom Avanto; Siemens Medical Solutions,

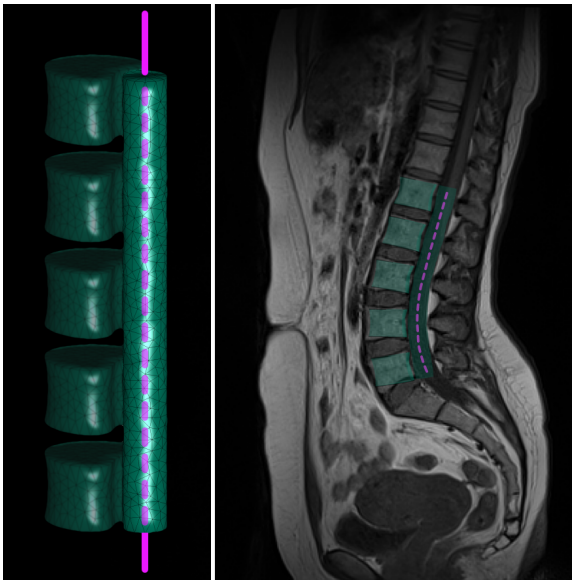

Figure 1: *The layered finite element model consists of more than 2,000 tetrahedrons (left). The spine canal center line is indicated by the dashed line. The model uses the image-induced potential field to align itself to find a local minimum after the initialization (right).*

Erlangen, Germany) by four trained technicians in a standardized way. Subjects were placed in the supine position. Five phased-array surface coils were placed to the head, neck, abdomen, pelvis, and lower extremities for whole-body imaging. The spine coil is embedded in the patient table. The spine protocol consisted of a sagittal T1-weighted turbo-spin-echo sequence (676 / 12 [repetition time msec / echo time msec]; 150° flip angle; 500 mm field of view; $1.1 \times 1.1 \times 4.0\,mm$ voxels) and a sagittal T2-weighted turbo-spin-echo sequence (3760 / 106 [repetition time msec / echo time msec]; 180° flip angle; 500 mm field of view; $1.1 \times 1.1 \times 4.0\,mm$ voxels). First, both sequences were placed over the cervical and upper thoracic spine. Then, they were placed over the lower thoracic and lumbar spine. The MRI software automatically composed a whole spine sequence from the two T1-weighted and T2-weighted sequences [HSS*13]. We were provided with 490 data sets.

Our work requires a detection of the lumbar spine in the MRI data. We employ a hierarchical finite element method according to [RET13]. Tetrahedron-based finite element models (FEM) of vertebrae and spinal canal are connected by a bar-shaped FEM (Fig. 1). The model comprises a fixed number of points which are pairwise relatable between instances of the model. Hence, correspondences between lumbar spine representations of different data sets can easily be established. The model is placed in the scene using an empirically chosen initialization point. The force acting on the model stems from aggregation of loads, which are derived from a potential field resulting from a weighted sum of the T1- and T2-weighted MRI images, see [RET13]. After detecting all spines, we register the models because in a later clustering step we only want to capture the local deformation of the lumbar spine, not different locations in world space. The models are registered using the Kabsch Algorithm [Kab76], which is designed to minimize the root mean squared deviation between paired sets of points. The model-based detection captures information about the spine canal curvature as well as the alignment of the vertebrae. It is not meant to capture information about vertebrae deformation and differences in spine canal extent.

5. Analysis of Lumbar Spine Canal Variability

We investigate the variability of the lumbar spine canal based on the deformed and registered models of the detection step. Since our primary interest is on the curvature of the spine, we focus on the spinal canal. Centerlines capture curvature and are easier to handle than the tetrahedral mesh. Clustering using Agglomerative Hierarchical Clustering is carried out to form groups that exhibit low intra-group and high inter-group shape variability. The clusters are visualized by means of representatives to reduce visual clutter and simplify a comparison between subgroups of the cohort.

5.1. Centerline Extraction

In this subsection, we describe how we compute the centerline $c_{\mathcal{S}}$ of the lumbar spine model $\mathcal{S}$. The model is given as a cylindrically shaped tetrahedral mesh. The axis of rotation is aligned to the z axis. Therefore, we use a parametric curve $c(t) = p_0 + t \cdot v_z$ where the z-component lies in $[h_{min}, h_{max}]$. Here, h_{min} and h_{max} are the minimal and maximal height of the mesh, respectively. We can write the parametric curve $c(t)$ as:

$$c(t) = \underbrace{\begin{pmatrix} 0 \\ 0 \\ h_{min} \end{pmatrix}}_{p_0} + t \cdot \underbrace{\begin{pmatrix} 0 \\ 0 \\ h_{max} - h_{min} \end{pmatrix}}_{v_z}, \qquad t \in [0,1]. \quad (1)$$

We determine the intersection points of the parametric curve with the faces of the tetrahedra $\tau \in \mathcal{S}$ of the undeformed lumbar spine model $\mathcal{S}_0$. Thus, we combine the vertices to obtain the triangles, faces and assess the intersection points with the curve. For this, we use vertices v_0, v_1, v_2, v_3 of every tetrahedra $\tau = \{v_0, v_1, v_2, v_3\}$ and solve the following matrix equation:

$$\begin{pmatrix} v_k & v_l & v_m & v_z \\ 1 & 1 & 1 & 0 \end{pmatrix} \cdot \begin{pmatrix} \alpha \\ \beta \\ \gamma \\ -t \end{pmatrix} = \begin{pmatrix} p_0 \\ 1 \end{pmatrix}, \qquad (2)$$

with different permutated $k, l, m \in \{0,1,2,3\}$ for the four different faces of the tetrahedra. The equation combines the

parametric curve with the triangle face according to barycentric coordinates to obtain the intersection point. If we obtain a positive solution $\alpha, \beta, \gamma > 0$, the considered curve point lies in the interior of a triangle of τ. Thus, we assign the corresponding tetrahedron with its triangle and their barycentric coordinates to the curve point $p_i = p_0 + t \cdot v_z$. If one curve point lies on the boundary of a triangle, i.e., one of the coordinates is equal to zero, we assign only one tetrahedron to the curve point. Using these values, we obtain the centerline of every deformed lumbar spine model by applying the stored barycentric coordinates to the corresponding tetrahedron. Having one intersection point p_i of the undeformed lumbar spine model with the assigned tetrahedra τ, the coresponding triangle face v_k, v_l, v_m, and the assigned barycentric coordinates α, β, γ, we extract the new point p_i' of the deformd lumbar spine model by applying:

$$p_i' = \alpha v_k + \beta v_l + \gamma v_m. \tag{3}$$

Hence, we gain the new centerline.

5.2. Centerline Clustering

To cluster the centerlines, we employ an Agglomerative Hierarchical Clustering (AHC) approach. It has been demonstrated that AHC delivers meaningful results in the clustering of other plane and space curves, such as fiber tracts from Diffusion Tensor Imaging (DTI) data [MVvW05], streamlines from flow data [YWSC12], and brain activation curves (time-series) from functional Magnetic Resonance Imaging (fMRI) data [LCYL08]. Furthermore, it is flexible with regard to cluster shape and size. AHC relies on the difference/similarity between data entities. Thus, a definition of centerline similarity is the prerequisite for AHC of centerlines.

Similarity is often evaluated by a distance measure. General requirements for such a measure are positive definiteness and symmetry. A valid example, that has been successfully employed for clustering fiber tracts and streamlines [MVvW05, YWSC12], is the *mean of closest point distances* (MCPD) proposed in [CGG04]. For two centerlines c_i and c_j with points p, the MCPD is computed as:

$$\begin{aligned} d_M(c_i, c_j) &= mean(d_m(c_i, c_j), d_m(c_j, c_i)) \\ with\ d_m(c_i, c_j) &= mean_{p_l \in c_i} \min_{p_k \in c_j} \|p_k - p_l\| \end{aligned} \tag{4}$$

Cluster Proximity. AHC requires beforehand the computation of all pairwise centerline distances and their storage in a quadratic and symmetric distance matrix **M**. The algorithm operates in a bottom-up manner. Initially, each centerline is considered as a separate cluster. The algorithm then iteratively merges the two closest clusters until a single cluster remains. The merge step relies on **M** and a measure of cluster proximity. Various cluster proximity measures have been published, among which *single link*, *complete link*, *average link*, and *Ward's method* [TSK05] are the most popular. In single link, the proximity of two clusters is defined as the minimum distance between any two centerlines in the different clusters. Complete and average link employ the maximum and the average of these distances, respectively. Ward's method aims at minimizing the total within-cluster variance at each iteration. It defines the proximity of two clusters as the sum of squared distances between any two centerlines in the different clusters (SSE: sum of squared errors). Before we elaborate on the most suitable proximity measure for our application, we focus on automatically computing a reasonable number of clusters k. This computation helps us in providing a good initial visual summary of the variants in spinal canal shape and it facilitates a more reproducible analysis.

Number of Clusters. Salvador and Chan propose a method for automatically computing the number of clusters in hierarchical clustering algorithms [SC04]. Their *L-method* is based on determining the *knee/elbow*, i.e., the point of maximum curvature, in a graph that opposes the number of clusters and a cluster evaluation metric. The knee is detected by finding the two regression lines that best fit the evaluation graph, and then, the number of clusters that is closest to their point of intersection is returned. Locating the knee depends on the shape of the graph, which again depends on the number of tested cluster numbers k. Salvador and Chan recommend using a full evaluation graph, which ranges from two clusters to the number of data entities. Starting with the full graph, the L-method is carried out iteratively on a decreasing focus region until the current knee location is equal to or larger than the previous location. As evaluation metric, the proximity measure used by the different link versions of AHC is applied. Furthermore, the evaluation is not based on the entire dataset but only on the two clusters that are involved in the current merge step.

Evaluation of Cluster Proximity Measures. In an informal evaluation based on 16 datasets, we tested AHC with the four proximity measures and the L-method. The 16 datasets represent the complete set of centerlines ($n = 490$) and epidemiologically relevant subsets derived according to gender, age, e.g. 20-40, 41-60 and 61-80, body weight, and body height. For each dataset, we applied the four proximity measures and visualized all clustering results side-by-side. A visual inspection of the results confirmed textbook knowledge with regard to the strengths and weaknesses of the proximity measures [TSK05] (Fig. 2 shows an exemplary scenario). In single link clustering, the *chaining effect* could be observed for every dataset. Here, a single large cluster arises containing almost the entire set of centerlines. This cluster contains very dissimilar centerlines but they are connected by a chain of similar ones via some transitive relationship. For the majority of datasets, average link failed to avoid this effect. Instead, strong outliers were represented as individual clusters while the remaining centerlines, being dissimilar and still comprising outliers, were grouped in a single

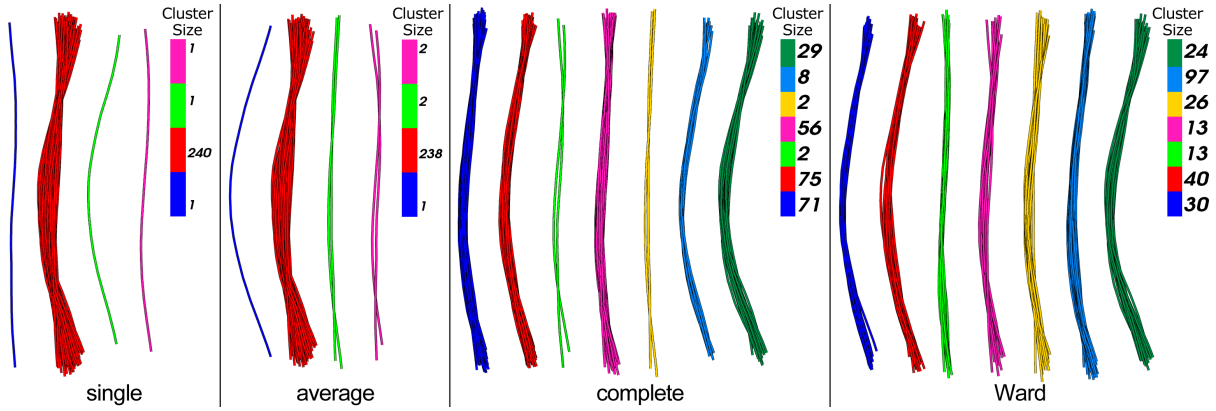

Figure 2: *Spinal canal centerlines of 242 female subjects clustered with Agglomerative Hierarchical Clustering using four different proximity measures and a technique for automatically computing the cluster count. Single link and average link suffer from the chaining effect (single large cluster), complete link produces compact, tightly bound clusters and Ward's method is biased towards generating clusters of similar size. The difference in centerline shape also occurs orthogonal to the view plane.*

large cluster. Complete link clustering produced small, compact, and tightly bound clusters. Ward's method was biased towards generating clusters with similar size. These clusters showed less diversity than the ones generated by means of complete link. In summary, due to the chaining effect of single link and average link, and the arbitrary assumption of similar cluster sizes in Ward's method, we favor complete link as a proximity measure.

The bottleneck of AHC in terms of time complexity is the computation of **M**, in particular when a multitude of closest point distances must be calculated (Eq. 4). However, our total number of centerlines ($n = 490$) and the number of vertices per centerline ($v = 93$) are relatively small. Furthermore, we have parallelized the computation and the matrix must be computed only once and may be stored. The computation of **M** based on the complete set of centerlines, i.e. the entire population, can be considered as the worst case. On a 3.07 GHz Intel 8-core PC with 8 GB RAM and a 64 bit Windows operating system, the computation took 7.9 *s*. The L-method for determining the number of clusters took 24.2 *s* and represents the bottleneck in processing our data. This is due to the multitude of computations required for finding the two best fit regression lines but may be mitigated by cutting off unlikely high numbers of clusters from the full evaluation graph [SC04].

The clustering implementation is based on the AHC algorithm and the proximity measures being part of MATLAB's Statistics Toolbox (MathWorks, Natick, MA, U.S.). The source code of the L-method is provided by A. Zagouras as part of MATLAB Central's file exchange [Zag].

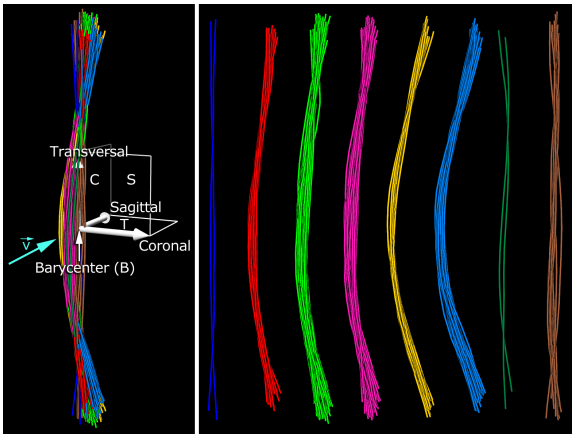

Figure 3: *Initially, all centerline clusters are closely intertwined (left). To simplify their interpretation, they are translated along the coronal axis and lined up at equidistant locations (right). The annotations illustrate typical medical view planes/axes: sagittal (S), coronal (C), and transversal (T). Our default viewing direction $\vec{v}$ is parallel to the sagittal axis (as can be seen in the right view).*

5.3. Visualization of Clustered Centerlines

A standard medical view for inspecting the spine in MR images is the sagittal view with the vertebrae located to the left of the spinal canal (Fig. 1, right). Hence, we choose it as the default view for the presentation of the clustering results. Initially, all centerlines and hence also the clusters, are closely intertwined in space due to the co-registration of all spine detection results (Sec. 4 and Fig. 3, left). In order to get a better overview of the individual clusters, they are translated

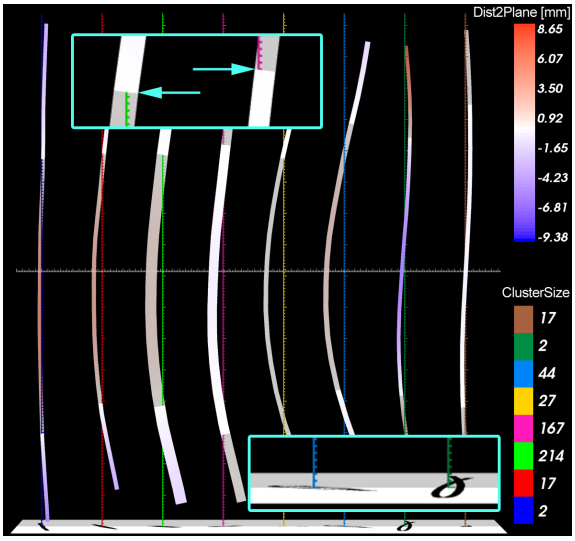

Figure 4: *Spinal canal centerlines of all subjects (n = 490) clustered with Agglomerative Hierarchical Clustering employing complete link. For each cluster, a representative centerline is visualized as a ribbon. Ribbon width encoded cluster size. Ribbon color encodes the distance to a view-aligned, highly transparent, sagittal plane passing through the barycenter B of the original centerline bundle (Fig. 3, left). The sequence of a ribbon's intersections with the plane supports an assessment of its curvature (upper inset). Shadow projections reveal how far a representative extends to either side of the plane (lower inset).*

along the coronal axis and lined up at equidistant locations (Fig. 3, right). The centerlines are visualized with GPU support as illuminated streamlines with halos [EBRI09]. The halos improve the visual separation of individual lines. Before the centerlines are translated, the barycenter B of the entire bundle of lines is computed (Fig. 3, left). It will be used for positioning visual hints in the scene.

Cluster Representatives. In order to simplify the interpretation of a cluster, to further reduce visual clutter, and to improve a visual comparison of clustering results between groups, e.g., younger and elder subjects, we compute a representative centerline for each cluster. This is inspired by the computation of a representative fiber tract for a bundle of fibers derived from DTI tractography data [BPHRA13]. Here, the fiber with the smallest sum of distances to all other fibers, i.e. the centroid fiber, of the bundle is chosen. Since all pairwise centerline distances are stored in $\mathbf{M}$, the selection of a centroid centerline is straightforward (Sec. 5.2). Each such centroid is then visualized by a ribbon whose width is scaled according to the size of the corresponding cluster (Fig. 4). Please note that the location of the vertebrae corresponding to this centroid centerline is intentionally not indicated since the ribbons are representative for the course of the spinal canal but not necessarily for the vertebrae location.

Visual Hints. The curvature of the spinal canal along the coronal axis is perceived well in the sagittal view. However, the curvature along the sagittal axis, i.e. the viewing direction, is only deducible by rotating the scene. Hence, we augment the sagittal view by three visual hints improving the curvature perception. (1) A highly transparent sagittal plane passing through B is added to the scene. The position of the ribbon parts with respect to the plane (in front/behind) and the visible intersections of ribbons and plane support the differentiation between spinal canals being mostly bended towards the viewer from those being bended away (Fig. 4, upper inset). (2) The ribbons are colored according to their distance to the sagittal plane. A diverging color scale is used to distinguish between parts in front of the plane (blue), close to the plane (white), and behind the plane (red). (3) A transversal plane is positioned below the ribbons and a light source is positioned above them. Shadow projections are computed and drawn on the plane. They provide an estimate of how far the representatives extend to either side of the plane (Fig. 4, lower inset). In some cases, the projections revealed subtle differences in shape, which could hardly be inferred from the other two hints.

Measurement and Interaction. In order to facilitate a more quantitative analysis of the centerlines and to support a comparison of individual representatives, a vertical and a horizontal axis including tick marks are added to each cluster representative (Fig. 4). All axes are located within the sagittal plane (1). An initial pair of axes running through B has been computed based on the entire set of centerlines and then copied and translated together with each cluster along the coronal axis (Fig. 3). The vertical axes are assigned a unique cluster color to interrelate the representatives and the cluster size legend. The interaction with the visualization exceeds standard 3D scene navigation. Individual representatives may be picked by the user and all centerlines of the corresponding cluster are visualized. The measurement of the spine based on neuralgic points is of crucial importance and has a long tradition in orthopedics. Hence, two measurement widgets have been added for measuring distances and angles (Fig. 5). Both widgets are bound to the geometry of the ribbons in order to simplify measurements in 3D space. The visualization has been implemented in C++ and the Visualization Toolkit. (Kitware, Inc., Clifton Park, NY, U.S.).

6. Results & Discussion

In this section, we present preliminary results combining our shape visualization with associated cohort study data. As seen in Fig. 4, the clustering step is a good way to detect outliers in the data as clusters with very few subjects that have an unusual shape. This can be utilized for finding pathological spine shapes–even for subjects, which do not have a diagnosed back disorder. The technique scales well

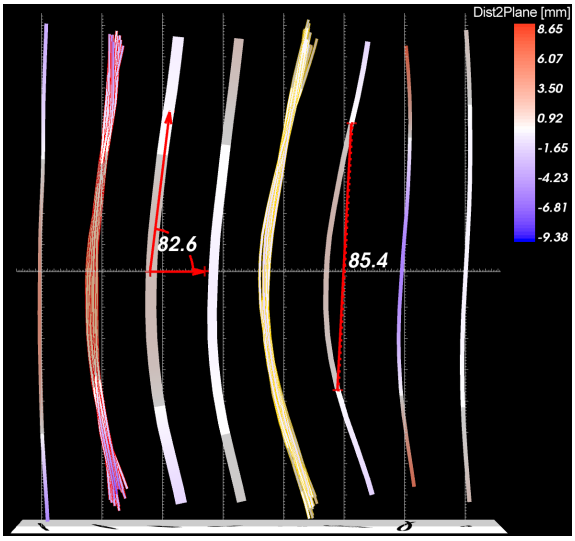

Figure 5: *Interaction facilities. The user may pick a cluster representative, i.e. a ribbon, causing the corresponding cluster to be visualized (centerlines with red and yellow halos). Widgets for measuring distances and angles facilitate a quantitative analysis of the spinal shape.*

regarding the number of input center lines. It is possible to generate an overview for hundreds of subjects as well as for smaller subsets, e.g. subjects which share certain similar attributes. A subset visualization can be applied to detect if the different shape clusters imply a significant difference in associated variables of interest. Does for example a physical demanding job correlate with an extraordinary curved spine?

Our clinical partners expected the lumbar spine to be more straight along the coronal axis for tall people, while being more sinuous ("*lordosis*") with decreasing body height. To check our results for medical plausibility, we created subsets of the data based on *body height*. For each cluster we calculated the distance to the arithmetic mean of *age*, *body height*, and *weight*. We computed the mean of the absolute lordosis curvatures K using the Frenet formulas [Fre52].

While the mean curvature K for people sized 150 – 160 cm is $38.99 \cdot 10^{-4}$ ($\sigma = 9.99 \cdot 10^{-4}$), it gets smaller the larger the subjects are, being at $34.59 \cdot 10^{-4}$ ($\sigma = 9.98 \cdot 10^{-4}$) for 160 – 170 cm and at $31.95 \cdot 10^{-4}$ ($\sigma = 8.88 \cdot 10^{-4}$) for 180 – 190 cm tall people. We could not only confirm the expected differences in the distinct groups, but also give clues for groups which share similar curvature. When looking at subject groups of body height 150 – 160 cm, 160 – 170 cm and 170 – 180 cm we always found a cluster of subjects which are about 10 years older than the rest of the group. They all presented a lordosis shape as well as an "S" shape in sagittal direction ("*scoleosis*"). Since a cluster showing the same characteristics was found in distinct subject groups, it is subject of further investigation.

This finding is an example of how a clustering result can create groups related by shape in order to find other correlations in the associated socio-economic and medical attribute parameters. It can also serve as starting point for a visual analytics tool to detect risk factors.

The visualization aims for at a visual comparability of the clusters. Additionally statistically reliable shape describing features would enhance the method by making statistical calculation applicable to deformation information. This can be achieved by storing the curvature and position of several fixed points in the FEM model. While the visualization allows for characterization of the lumbar spine curvature, it is currently not possible to predicate information about spinal canal narrowings, which can also be an indicator for pathologies like spinal stenosis. This is also the case for a vertebrae deformation, which is an indicator for osteoporosis. We plan to incorporate such information, e.g, based on an extension of the finite element model used for spine detection.

7. Conclusion & Future Work

Applying analysis of medical image data associated with non-image data in a cohort study context is both promising and challenging. The multitude of subjects requires robust yet precise and at least semi-automatic detection and segmentation algorithms which capture the shape of a structure of interest over a large space of subjects. Assessing the resulting information space demands visualizations, which map relevant information among large groups of subjects.

We aim to include more shape describing metrics and apply the technique to all cohort study subjects. This allows for a statistically reliable comparison of clusters. Currently, only the overall curvature and torsion is calculated. Those can be misleading metrics, since coronal as well as sagittal deformation can induce a large curvature. The deformation should be class-divided with the analyzed pathology in mind. Those and other morphology describing metrics can be transferred to the cohort study data dictionary. We also want to include information about unusual vertebrae alignment.

Our presented approach implements a pipeline for analyzing the lumbar spine canal in order to correlate its shape to other variables associated with the cohort study. This was done using an association to *body height*, *gender*, *age* and *weight*. While this was a first step to confirm the expected shape in different subject groups, it has to be enhanced to be applicable to all data variables measured in the cohort.

We plan a web-based visual analytics framework that allows for information visualization on non-image data in combination with complex data set queries including the shape of structures. This allows for possibilities to support queries which are not easy to make in classic statistics

software, like filtering by geographic location as closeness to the coast. We want to provide the epidemiologists with a fast and effective way to analyze their data sets exploiting the potential which lies beneath the numbers.

Acknowledgements: SHIP is part of the Community Medicine Research net of the University of Greifswald, Germany, which is funded by the Federal Ministry of Education and Research (grant no. 03ZIK012), the Ministry of Cultural Affairs as well as the Social Ministry of the Federal State of Mecklenburg-West Pomerania. Whole-body MR imaging was supported by a joint grant from Siemens Healthcare, Erlangen, Germany and the Federal State of Mecklenburg-Vorpommern. The University of Greifswald is a member of the 'Centre of Knowledge Interchange' program of the Siemens AG. This work was supported by the DFG Priority Program 1335: Scalable Visual Analytics.

References

[BBP10] BUSKING S., BOTHA C., POST F.: Dynamic Multi-View Exploration of Shape Spaces. *Computer Graphics Forum 29*, 3 (2010), 973–982. 2

[BPHRA13] BRECHEISEN R., PLATEL B., HAAR ROMENY B., A. V.: Illustrative uncertainty visualization of DTI fiber pathways. *The Visual Computer 29*, 4 (2013), 297–309. 6

[CGG04] COROUGE I., GOUTTARD S., GERIG G.: Towards a shape model of white matter fiber bundles using diffusion tensor mri. In *IEEE International Symposium on Biomedical Imaging: Nano to Macro, 2004.* (2004), pp. 344–347 Vol. 1. 4

[CLA*09] CHOU Y.-Y., LEPORÉ N., AVEDISSIAN C., MADSEN S. K., PARIKSHAK N., HUA X., SHAW L. M., TROJANOWSKI J. Q., WEINER M. W., TOGA A. W., THOMPSON P. M., ALZHEIMER'S DISEASE NEUROIMAGING INITIATIVE: Mapping correlations between ventricular expansion and CSF amyloid and tau biomarkers in 240 subjects with Alzheimer's disease, mild cognitive impairment and elderly controls. *NeuroImage 46*, 2 (June 2009), 394–410. 2

[CRY11] CABAN J. J., RHEINGANS P., YOO T.: An Evaluation of Visualization Techniques to Illustrate Statistical Deformation Models. *Computer Graphics Forum 30*, 3 (2011), 821–830. 2

[EBRI09] EVERTS M. H., BEKKER H., ROERDINK J. B., ISENBERG T.: Depth-dependent halos: Illustrative rendering of dense line data. *IEEE Trans. Vis. Comput. Graphics 15*, 6 (2009), 1299–1306. 6

[Fre52] FRENET F.: Sur les courbes à double courbure. *Journal de Mathématiques Pures et Appliquées* (1852), 437–447. 7

[HSK11] HERMANN M., SCHUNKE A. C., KLEIN R.: Semantically steered visual analysis of highly detailed morphometric shape spaces. In *BioVis 2011: 1st IEEE Symposium on biological data visualization* (Oct. 2011), pp. 151–158. 2

[HSS*13] HEGENSCHEID K., SEIPEL R., SCHMIDT C. O., VÖLZKE H., KÜHN J.-P., BIFFAR R., KROEMER H. K., HOSTEN N., PULS R.: Potentially relevant incidental findings on research whole-body MRI in the general adult population: frequencies and management. *European Radiology 23*, 3 (2013), 816–826. 2, 3

[Kab76] KABSCH W.: A solution for the best rotation to relate two sets of vectors. *Acta Crystallographica Section A 32*, 5 (Sep 1976), 922–923. 3

[LCYL08] LIAO W., CHEN H., YANG Q., LEI X.: Analysis of fMRI Data Using Improved Self-Organizing Mapping and Spatio-Temporal Metric Hierarchical Clustering. *IEEE Transactions on Medical Imaging 27*, 10 (2008), 1472–1483. 4

[LTERAC11] LANG-TAPIA M., ESPAÑA-ROMERO V., ANELO J., CASTILLO M.: Differences on spinal curvature in standing position by gender, age and weight status using a noninvasive method. *J Appl Biomech 27*, 2 (2011), 143–50. 2

[MM05] MANEK N. J., MACGREGOR A. J.: Epidemiology of back disorders: prevalence, risk factors, and prognosis. *Current opinion in rheumatology 17*, 2 (Mar. 2005), 134–140. 2

[MVvW05] MOBERTS B., VILANOVA A., VAN WIJK J.: Evaluation of Fiber Clustering Methods for Diffusion Tensor Imaging. In *IEEE Visualization* (2005), pp. 65 – 72. 4

[RET13] RAK M., ENGEL K., TÖNNIES K. D.: Closed-Form Hierarchical Finite Element Models for Part-Based Object Detection. In *Vision, Modeling, Visualization* (2013). 3

[RFS03] RUECKERT D. D., FRANGI A. F. A., SCHNABEL J. A. J.: Automatic construction of 3-D statistical deformation models of the brain using nonrigid registration. *IEEE Transactions on Medical Imaging 22*, 8 (July 2003), 1014–1025. 2

[SC04] SALVADOR S., CHAN P.: Determining the Number of Clusters/Segments in Hierarchical Clustering/Segmentation Algorithms. In *Proc. of Tools with Artificial Intelligence. ICTAI* (2004), pp. 576 – 584. 4, 5

[SMvB*10] STEENWIJK M., MILLES J., VAN BUCHEM M., REIBER J. H. C., BOTHA C.: Integrated Visual Analysis for Heterogeneous Datasets in Cohort Studies. *Proc. of IEEE VisWeek Workshop on Visual Analytics in Health Care* (2010). 2

[SWST03] SCHULZE-WOLLGAST P., SCHUMANN H., TOMINSKI C.: Visual analysis of human health data. *International Resource Management Association, Philadelphia* (2003). 2

[TSK05] TAN P.-N., STEINBACH M., KUMAR V.: *Introduction to Data Mining*. Addison Wesley, 2005. 4

[TYO*09] TUCER B. B., YALCIN B. M. B., OZTURK A. A., MAZICIOGLU M. M. M., YILMAZ Y. Y., KAYA M. M.: Risk factors for low back pain and its relation with pain related disability and depression in a Turkish sample. *Turkish Neurosurgery 19*, 4 (Sept. 2009), 327–332. 2

[VAS*11] VÖLZKE H., ALTE D., SCHMIDT C., ET AL.: Cohort Profile: The Study of Health in Pomerania. *International Journal of Epidemiology 40*, 2 (Mar. 2011), 294–307. 1

[vLBK*13] VON LANDESBERGER T., BREMM S., KIRSCHNER M., WESARG S., KUIJPER A.: Visual analytics for model-based medical image segmentation: Opportunities and challenges. *Expert Systems with Applications 40*, 12 (2013), 4934–4943. 2

[vTKB02] VAN TULDER M., KOES B., BOMBARDIER C.: Low back pain. *Best Practice & Research Clinical Rheumatology 16*, 5 (2002), 761 – 775. 1, 2

[WP03] WOOLF A. D., PFLEGER B.: Burden of major musculoskeletal conditions. *Bulletin of the World Health Organization 81*, 9 (2003), 646–656. 1

[YWSC12] YU H., WANG C., SHENE C.-K., CHEN J. H.: Hierarchical Streamline Bundles. *IEEE Transactions on Visualization and Computer Graphics 18*, 8 (2012), 1353–67. 4

[Zag] A. Zagouras. L-method for Computing the Optimal Number of Clusters. www.mathworks.com/matlabcentral/fileexchange/37295-l-method/content/Lmethod.m. 5

[ZGP12] ZHANG Z., GOTZ D., PERER A.: Interactive Visual Patient Cohort Analysis. *Proc. of IEEE VisWeek Workshop on Visual Analytics in Healthcare, Seattle, Washington* (2012). 2